Macromolecular Chemistry and Physics
www.mcp-journal.de

Impact of Comonomer Chemistry on Phase Behavior of Polymerizable Lyotropic Ionic Liquid Crystals: A Pre- and Post-Polymerization Study

Nicolas Goujon, Ludovic F. Dumée, Nolene Byrne, Gary Bryant, and Maria Forsyth*

The design and characterization of polymerizable lyotropic ionic liquid crystals with an intact alkyl chain bilayer are described. The bilayer is left intact to enable further inclusion of peptide-based channels to mimic biological protein membranes for potential separation applications. Impact of comonomer concentration and chemistry on the mesophase formed pre- and post-polymerization is characterized. An optimum comonomer concentration of 20 wt% is found for the poly(ethylene glycol) diacrylate (PEGDA) system, before full disruption of the discontinuous cubic phase occurs. Little impact on the discontinuous cubic phase is observed by varying comonomer chemistry from PEGDA to either poly(ethylene glycol) dimethacrylate or 2-hydroxyethyl acrylate, with exception of variation in the thermal stability of the resulting mesophase. Surprisingly, the use of 2-hydroxyethyl methacrylate as comonomer results in formation of the 2D hexagonal phase, which is of interest for the design of biological protein membranes. Unfortunately, mesostructure retention is not observed in any systems studied. A sequence of structural changes, modeled as a change from a spherical micelle to a cylindrical micelle, and to finally a lamellar architecture, is rather observed using in situ small-angle X-ray scattering polymerization measurements, suggesting a reduction of the headgroup area, likely caused by cross-linking of the acrylate moiety.

1. Introduction

The development of polymeric membranes with highly ordered nanostructure has attracted a great deal of interest for their potential application in drug delivery, energy devices, and separation.[1–4] Such materials may display unique properties, including 3D-interconnected conducting channels (e.g., bicontinuous cubic phase) and anisotropic transport properties (e.g., 2D-hexagonal phase), making them relevant for individual molecule diffusion.[3,5,6] To date, various design approaches have been reported for the fabrication of highly ordered nanostructured polymeric membranes, including the use of block copolymer,[7,8] polymerizable thermotropic liquid crystal,[5,9] or polymerizable lyotropic liquid crystal (LLC).[10]

The LLC self-assembly method offers the advantage that the mesophase can be tailored prior to polymerization to target specific application needs.[11] Such lyotropic liquid crystalline phases are formed by spontaneous self-assembly of amphiphilic molecules via the addition of a cosolvent such as water or alcohol[11–13] Depending on the nature and concentration of the cosolvent, a wide variety of mesophases may be generated, including lamellar, 2D-hexagonal and discontinuous or bicontinuous cubic phases.[11]

Additionally, the alkyl chain bilayer formed by some LLC systems is quite similar to biological membrane, which could unlock the use of peptide-based channels as ion/molecule carriers in a polymeric membrane.[14] Peptide-based channels, such as cyclic peptide nanotubes (CPNs) represent an elegant way to selectively transport ions/molecules via size exclusion or inner wall functionalization.[15–17] Briefly, CPNs consist of a cyclic amino acid sequence which can self-assemble into tubular architecture via hydrogen bonding. CPNs with inner diameter ranging from 5.9 to 13.1 Å can be readily achieved by selecting the number of amino acid subunits.[18] The fabrication of sub-nanometer porous membranes remains challenging using conventional techniques,[2] and therefore the design of a biological membrane using a polymerizable LLC system in conjunction with CPNs could potentially help to overcome current fabrication limitations. Recently, we showed that the nanostructured domains presented in LLC systems could be used to align CPNs in a similar manner to that of protein membranes in biological membrane.[19]

Unfortunately, the poor mechanical properties of LLC systems, due to their gel-like nature, have hindered their implementation.[20,21] As mentioned previously, the mesophases formed by LLC systems are extremely sensitive to cosolvent

Dr. N. Goujon, Dr. L. F. Dumée, Dr. N. Byrne, Prof. M. Forsyth
Institute for Frontier Materials, Deakin University—Geelong
Waurn Ponds, Victoria 3216, Australia
E-mail: nicolas.goujon@deakin.edu.au
Prof. G. Bryant
Centre for Molecular and Nanoscale Physics
School of Applied Sciences
RMIT University
GPO Box 2476, Melbourne, Victoria 3001, Australia
Prof. M. Forsyth
ARC Centre of Excellence for Electromaterials Science
Institute for Frontier Materials
Deakin University
Burwood, Victoria 3125, Australia
The ORCID identification number(s) for the author(s) of this article can be found under https://doi.org/10.1002/macp.201800307.

DOI: 10.1002/macp.201800307

concentration, which is an advantage for design flexibility but also a key challenge in terms of mesophase thermal stability.[20,22] The use of ionic liquids with very low vapor pressures as cosolvents has already been suggested to improve the thermal stability of an LLC mesophase.[23,24] Mechanical stability remained a concern since the LLC mesophases formed with ionic liquids are still gel-like materials. A promising alternative, which could address both thermal stability and mechanical integrity simultaneously, lies in the development of photopolymerized LLC systems, whereby long-range order is retained after UV-polymerization.[7,25,26] Photopolymerized LLC systems reported so far can be categorized into two subclasses where: i) an LLC system is used as a pore former and is subsequently removed post-polymerization, resulting in the formation of nanoscale porosity[25,27,28] or where ii) a polymerizable LLC is used and covalently bonded to the polymer backbone. The latter case allows the amphiphile to be used as a permanent scaffold for the incorporation of host molecules, particles, and peptide-based channels.[14,29]

The main challenge regarding the development of a polymerizable LLC system is the retention of the mesostructure post-photopolymerization. Most polymerizable LLCs reported to date belong to the class of charged surfactants, including anionic-based surfactants[14,30–32] (e.g., sodium undecenoate, imidazolium-based ionic liquids), hydrated lipids[33–35] (e.g., phosphoethanolamine), cationic-based surfactants[36–38] (e.g., imidazolium and phosphonium-based ionic liquids), and gemini-based surfactants[39] (e.g., phosphonium-based ionic liquids). All confirmed cases of mesostructure retention have been reported for LLC systems where polymerizable moieties were located on the surfactant alkyl chain.[31–36,39] Attempts of LLC photopolymerization, where the polymerizable moiety was located at the counterion or associated with the cation headgroup[29] of an imidazolium-based ionic liquid, have been reported by Firestone et al. However, these LLC systems underwent phase rearrangement toward mesostructure with lower spontaneous curvature during photopolymerization. Phase rearrangement was also reported for another imidazolium-based ionic liquid where the polymerizable moiety was this time located on the surfactant alkyl chain.[37] Interestingly, the common feature of all these imidazolium-based ionic liquids was their relatively short alkyl chain (≤10 carbons) compared to that of traditional surfactants. The short alkyl chain length of the amphiphile might have weakened the nano-segregation of the hydrophilic/hydrophobic domains in these systems.[40] The change in balance between hydrophilic and hydrophobic domains in that case might have contributed to a detrimental effect on the mesostructure retention of these systems during photopolymerization. Building upon prior work from Firestone et al., a polymerizable lyotropic ionic liquid crystal with a longer alkyl chain (hexadecyl) was recently designed by our group, and its phase behavior upon addition of water determined.[41] In this work, an imidazolium-based ionic liquid with a polymerizable moiety located on the counterion (i.e., acrylate ion, as per Firestone et al. work[14]) was selected to limit the disruption of the alkyl chain bilayer for the incorporation of host molecules, particles, or peptide-based channels.[14]

Herein, the development of a polymerizable LLC system using a polymerizable lyotropic ionic liquid crystal, 1-hexadecyl-3-methylimidazolium acrylate (C_{16}mimAcr, **Figure 1**a) is described and characterized. For fabrication of an LLC copolymer network, a comonomer is often required for the production of a self-standing membrane.[14,42] Therefore, the impact of the comonomer chemistry and concentration on the phase behavior of the C_{16}mimAcr/water/comonomer systems was characterized prior and post-polymerization. In situ small-angle X-ray scattering (SAXS) polymerization assays were also performed on selected LLC systems to give real-time insights on the structural rearrangement occurring in these systems during photopolymerization. This study aims to give insights on the key parameters required for the development of sustainable peptide-based polymeric membrane using polymerizable LLC, in particular, the importance of the location of the polymerizable moiety and comonomer chemistry on the mesostructure retention of polymerizable LLC during photopolymerization.

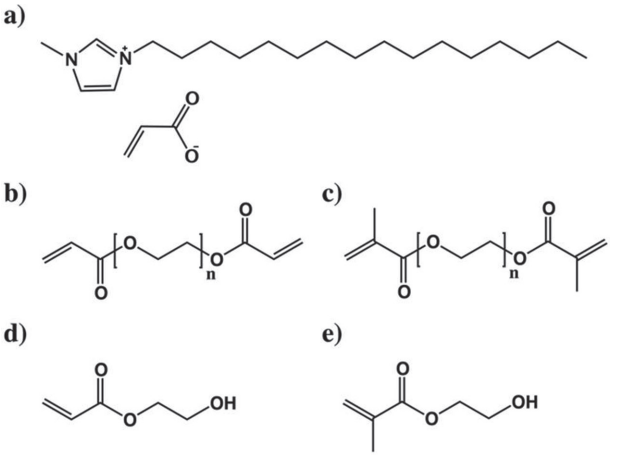

Figure 1. a) Chemical structure of the polymerizable lyotropic ionic liquid crystal, 1-hexadecyl-3-methylimidazolium acrylate (C_{16}mimAcr) and the comonomers investigated: b) poly(ethylene glycol) diacrylate (PEGDA, M_n: 575), c) poly(ethylene glycol) dimethacrylate (PEGDMA, M_n: 400), d) 2-hydroxyethyl acrylate (HEA), and e) hydroxyethyl methacrylate (HEMA).

2. Experimental Section

2.1. Chemicals and Materials

1-methylimidazole (99%), acrylic acid (99%), cyclohexane (≥99%), poly(ethylene glycol) diacrylate (M_n = 575), 2-hydroxyethyl acrylate (96%), 2-hydroxyethyl methacrylate (97%), 2-hydroxy-2-methylpropiophenone (97%), and Amberlyst-26 OH form were purchased from Sigma-Aldrich (New South Wales, Australia). Poly(ethylene glycol) dimethacrylate (M_n = 400) was purchased from Polysciences Inc (Taipei, Taiwan). 1-chlorohexadecane (97%) was purchased from Alfa Aesar (New South Wales, Australia). All chemicals were used as received.

1.5 mm outer diameter special glass 10 capillaries were purchased from Hampton Research Corporation. Quartz coverslips (25.4 × 25.4 square mm) were purchased from ProSciTech (Victoria, Australia).

2.2. Ionic Liquid Synthesis

2.2.1. 1-Hexadecyl-3-methyl-imidazolium Chloride (C_{16}mimCl)

C_{16}mimCl was synthesized according to the following procedure. In a 250 mL round bottom flask equipped with magnetic stirrer and a water-cooling system, 1-methylimidazole (11.96 g, 0.1458 mol) and 1-chlorohexadecane (43.13 g, 0.160 mol) were added simultaneously. Then the mixture was stirred at 80 °C for 72 h under a nitrogen atmosphere resulting in a slightly yellow solid. The product was purified by recrystallizing twice from ethyl acetate. Finally, the pure C_{16}mimCl was dried under high vacuum at 50 °C for 8 h resulting in a white powder product.

^{1}H NMR (500 MHz; DMSO-d_6, δ): 9.49 (s, 1H), 7.86 (s, 1H), 7.80 (s, 1H), 4.18 (t, 2H), 3.87 (s, 3H), 1.75 (m, 2H), 1.20 (m, 26H), 0.82 (t, 3H).

2.2.2. 1-Hexadecyl-3-methyl-imidazolium Acrylate (C_{16}mimAcr)

Anion exchange step used in this work differs from the procedure previously reported by Firestone et al.,[14] where silver acrylate salts were used. It was found to be quite difficult to remove the silver bromide product by filtration due to the small particle size of the silver bromide. As a consequence, the use of an ion exchange resin for the anion exchange step was preferred, as it avoids the presence of silver bromide impurity and the procedure is described below.

First, 300 g of ion exchange resin (Amberlyst-26 OH form) was loaded with the desired acrylate anion using a 10 wt% acrylic acid solution (1000 mL). The resin was then washed with an abundant amount of Milli-Q water to remove the unreacted acrylic acid residue. 30.03 g of 1-hexadecyl-3-methyl-imidazolium chloride was dissolved in 100 mL of Milli-Q water and the aqueous solution of ionic liquid was flushed through the column ten times (anion exchange yield was assessed by ^{1}H NMR). The acrylate-based ionic liquid was concentrated and dried under high vacuum resulting in a slightly yellow gel-like material. The product was purified by recrystallizing twice from ethyl acetate. Finally, the pure C_{16}mimAcr was dried under high vacuum at 30 °C for 8 h resulting in a white powder product.

^{1}H NMR (500 MHz; DMSO-d_6, δ): 9.71 (s, 1H), 7.84 (s, 1H), 7.77 (s, 1H), 5.97–5.92 (dd, 1H), 5.69–5.66 (dd, 1H), 5.13–5.10 (dd, 1H), 4.17 (t, 2H), 3.87 (s, 3H), 1.75 (m, 2H), 1.21 (m, 26H), 0.82 (t, 3H).

2.3. Lyotropic Liquid Crystalline Phase Preparation

2.3.1. Ionic Liquids/Water/Comonomer Systems

Each lyotropic liquid crystalline phase was prepared by weighing the appropriate amount of C_{16}mimAcr into a 4 mL glass vial. Residual water present in the C_{16}mimAcr was assessed using a Karl fisher method, via dissolving the C_{16}mimAcr into a methanol solution with a known water content. The amount of water already present in the C_{16}mimAcr was taken into consideration for the preparation of the lyotropic liquid crystalline phase. The desired amounts of Milli-Q water and comonomer were added according to their respective densities using a micropipette. Each mixture was first sonicated for several hours as a premixing step. Then the mixture was heated into their fluid state (90 °C) for a brief moment and mixed using a vortex agitator (avoiding the formation of bubbles). For the polymerization study, the photoinitiator was added after this step, by melting again the LLC phases into their fluid state (90 °C) for a brief moment and mixed using a vortex agitator.

To study the impact of comonomer concentration, C_{16}mimAcr/water/PEGDA systems with the following formulation were prepared: 35/65/0, 35/60/5, 35/55/10, 35/45/20, 35/35/30 wt%.

To study the impact of comonomer chemistry, C_{16}mimAcr/water/comonomer systems with a formulation of 35/45/20 wt% were prepared.

2.4. Polymerization of Lyotropic Liquid Crystal Systems

For the polymerization study, all lyotropic liquid crystalline phases were doped with 2 wt% of a radical photoinitiator, 2-hydroxy-2-methylpropiophenone. The lyotropic mesophases were sandwiched between two standard coverslips with a 250 μm-thick PTFE spacer. Polymerization temperature was controlled using a linkam stage equipped with quartz windows (Linkam Scientific LTS350). All lyotropic mesophases were photopolymerized using a high-pressure mercury UV lamp with sample-lamp distance of ≈15 cm (irradiance intensity of 89 mW cm^{-2} at 15 cm for UVC range (250–260 nm) without any filter or coverslip). The UV-exposure times were varied from 30 min to 3 h, depending on the UV-exposure times required for each C_{16}mimAcr/water/comonomer system to form a self-standing polymer film. It is important to note that some C_{16}mimAcr/water/comonomer system did not form a self-standing polymer film, even after 3 h of UV-exposure (see Supporting Information for details).

2.5. SAXS/WAXS

2.5.1. Benchtop SAXS/WAXS Setup

SAXS and wide-angle X-ray scattering (WAXS) measurements were recorded with a microcalix SAXS system (Bruker) using Cu Kα radiation (50 kV, 10 mA). The scattering vector, q, was calibrated using silver behenate. Prior to polymerization, the samples were placed into 1.5 mm outer diameter capillaries (special glass #10). For the polymer sample, the samples were mounted directly on a solid sample holder. Measurements were carried out under vacuum at 20 °C with exposure times of 600 or 2400 s for the gel sample and the polymer sample, respectively. For the C_{16}mimAcr/water/comonomer system containing 20 wt% comonomer, SAXS patterns were also collected at 40, 60, 80, and 90 °C, in order to assess the melting point of the lyotropic mesophase. The program Fit2D was used to extract the 1D-SAXS profile (i.e., intensity vs scattering vector, $q = (4\pi \sin \theta)/\lambda$), both presented on a logarithmic scale. The data were not corrected for the scattering from an empty capillary since the SAXS data were only analyzed

crystallographically.[11] The broad peak observed at 0.4 Å^{-1} is caused by the Kapton windows of the capillary holder and does not affect data interpretation. No Kapton windows were used for the solid sample holder, thus no peak Kapton was observed for the polymer sample.

2.5.2. Synchrotron SAXS/WAXS Setup

In situ SAXS polymerization measurements were performed at the Australian Synchrotron on the SAXS/WAXS beamline. An in-vacuum undulator (22 mm period, 3 m length, K_{max} = 1.56) with a beam energy of 20 keV and a 0.9 m camera length were used, allowing a detection range for a momentum transfer of 0.03 Å^{-1} < q < 1.5 Å^{-1}. The scattering vector, q, was calibrated using silver behenate. The 2D SAXS patterns were recorded with a 1M Pilatus detector with 981 × 1043 pixel resolution.[43]

A similar polymerization protocol, as described above, was used for the in situ SAXS polymerization measurement. SAXS patterns were recorded every 18 s.

2.6. Differential Scanning Calorimetry

DSC measurements were performed on an NETZSCH DSC 214 polyma instrument, which was calibrated using cyclohexane. The samples were accurately weighed (20–40 mg) into standard sealed aluminum pans. The weights of the pans containing the samples were measured before and after the DSC measurement to determine eventual weight loss, which was attributed to water loss. The samples were heated from 173.15 to 363.15 K and then cooled down from 363.15 to 173.15 K at the rate of 10 K min^{-1}. Isothermal steps of 5 and 2 min were added at 173.15 and 363.15 K, respectively. This cycle was repeated three times.

3. Results and Discussion

The incorporation of a comonomer into the LLC mesophase formed by C_{16}mimAcr/water system is likely to induce some structural disruptions that could affect either the thermal stability of the present mesophase or to even greater extent the type of mesophase formed. On the other hand, it was also found that the concentration of comonomer (i.e., PEGDA) has a significant impact on the resulting mechanical properties of the polymerized LLC membrane, with higher comonomer concentration resulting in the fabrication of self-standing LLC polymer film at a given UV-exposure time (30 min, see Supporting Information for details). Therefore, the comonomer concentration needs to be precisely controlled in order to produce self-standing LLC polymer film without sacrificing the formation of the mesophase. Additionally, the chemical properties of the comonomer are an important parameter, where parameters such as the type of polymerizable moiety, the number of polymerizable moieties per comonomer molecule, and the hydrophilic nature of the comonomer can all play a role in impacting the polymerization kinetics, cross-linking density, and resulting physical properties of the films.

To study these effects on this polymerizable LLC system (i.e., C_{16}mimAcr), the following comonomers have been selected to explore the impact of comonomer chemistry: poly(ethylene glycol) diacrylate (PEGDA, M_n: 575 g mol^{-1}), poly(ethylene glycol) dimethacrylate (PEGDMA, M_n: 400 g mol^{-1}), 2-hydroxyethyl acrylate (HEA), and hydroxyethyl methacrylate (HEMA). The chemical structure of the polymerizable LLC and the different comonomers used in this study are presented in Figure 1.

3.1. Pre-Photopolymerization Characterization

First, the impact of comonomer concentration on the phase behavior and thermal stability of the mesophase formed by the C_{16}mimAcr/water/PEGDA systems was investigated by means of SAXS and DSC, using the PEGDA comonomer, due to the fast polymerization kinetics of this system (see Supporting Information). The C_{16}mimAcr/water system containing 65 wt% water was selected for this study, as water evaporation was occurring prior to the melt at composition containing lower water concentration.

3.1.1. Impact of PEGDA Comonomer Concentration

The impact of PEGDA incorporation was investigated by substituting a portion of the water originally present in the C_{16}mimAcr/water system (35/65 wt%) with up to 30 wt% of PEGDA. **Figure 2** shows the SAXS profiles of C_{16}mimAcr/water/PEGDA as a function of PEGDA concentration. As previously reported, the C_{16}mimAcr/water system containing 65 wt% water exhibits a SAXS pattern characteristic of a discontinuous cubic phase, which could be properly indexed as a $Pm\bar{3}n$ space group.[41] The discontinuous cubic phase is observed for all PEGDA concentrations up to 20 wt%; it was also indexed as a $Pm\bar{3}n$ lattice, with up to 15 identified reflections for the sample containing 20 wt% PEGDA. As PEGDA concentration

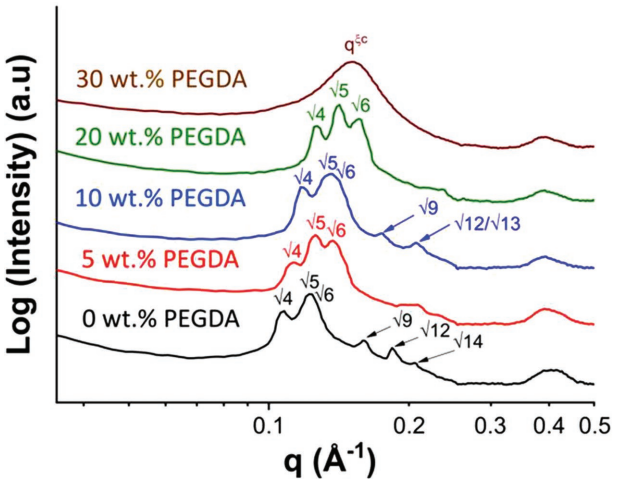

Figure 2. Integrated lab-SAXS patterns of C_{16}mimAcr/water/PEGDA systems containing: 35/6/0 wt% (black), 35/60/5 wt% (red), 35/55/10 wt% (blue), 35/45/20 wt% (green), and 35/35/30 wt% (brown). Peak assignment for the main diffraction peaks is also included (arrows).

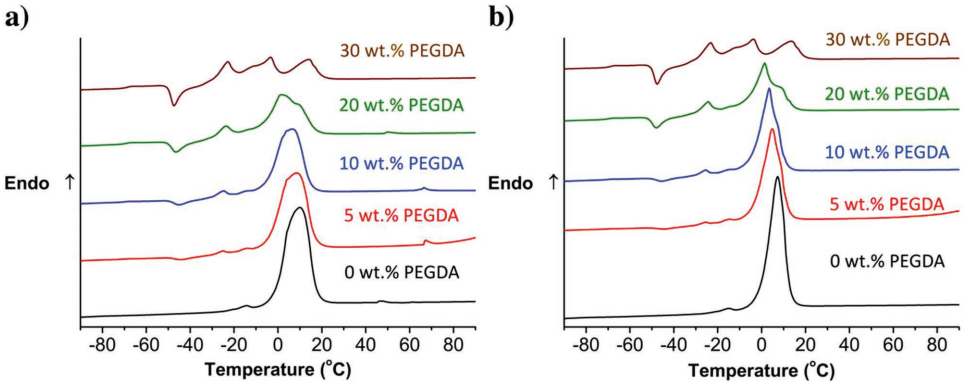

Figure 3. DSC heating profiles of the C_{16}mimAcr/water/PEGDA system containing: 35/65/0 wt% (black), 35/60/5 wt% (red), 35/55/10 wt% (blue), 35/45/20 wt% (green), and 35/35/30 wt% (brown); a) First heating scan and b) second heating scan.

increased up to 20 wt%, the SAXS pattern gradually shifted to higher q values, suggesting that the lattice parameter, a, of the discontinuous cubic phase is decreasing (see Table S3, Supporting Information). This decrease in a is probably related to the water layer around each micelle, which shrinks as the global amount of water is reduced. Polar fragrance compounds solubilized into a discontinuous cubic phase previously also showed a strong tendency to be located at the headgroup interface, causing a reduction of the lattice parameter.[44,45] Therefore, it could be assumed that the PEGDA molecules are located at the headgroup interface due to its hydrophilic nature, and thus, contributing to the reduction in a. At 30 wt% PEGDA, the SAXS pattern of the system changes drastically and an intermicelle interference peak centered at $q \approx 0.15$ Å^{-1} appears, indicating the formation of an isotropic micellar solution. This new peak corresponds to the correlation length of the pair distribution function of micelles, $\xi_c = 41.7$ Å (from $q = 2\pi/\xi_c$).[22,46]

Figure 3 shows the DSC profiles of the C_{16}mimAcr/water/PEGDA system as a function of PEGDA concentration. All PEGDA concentrations are highly viscous and transparent materials that do not flow, with the exception of the 30 wt% PEGDA which was liquid and transparent at room temperature. Below 30 wt% PEGDA, the main endothermic event between 0–4 °C appears more resolved during the second heating scan. This is likely due to difference in thermal history of the sample as a relatively slow cooling rate of 10 °C min^{-1} is used between cycles. Unless specified, DSC discussion in this section refers to the second heating scan.

The C_{16}mimAcr/water system containing 65 wt% water exhibits a sharp endothermic peak around 4 °C with a higher temperature shoulder.[41] As previously reported, the main transition corresponds to the lamellar crystalline phase to lamellar gel phase transition, while the higher temperature shoulder endothermic transition is likely to be a lamellar gel phase to discontinuous cubic phase transition, in this case.[22,41] As PEGDA is incorporated into the system, this higher temperature shoulder becomes more pronounced and gradually shifts to higher temperature with increasing PEGDA concentration, suggesting that PEGDA addition stabilizes the lamellar gel phase present after the crystallization of these systems, below 13 °C.[22] At 30 wt% PEGDA, this transition finally becomes a distinct endothermic event, observed at 13 °C, which corresponds to the melting into an isotropic liquid. Simultaneously, the main endothermic event shifts from 4 to −3 °C as PEGDA concentration increases, suggesting this time that the thermal stability of the lamellar crystalline phase decreases. Additionally, a glass transition around −69 °C and a crystallization event around −47 °C, likely associated to the ethylene oxide chains, become more apparent as the PEGDA concentration is increased.

A noticeable difference between the first and second heating scans for the samples containing up to 20 wt% PEGDA is the appearance of a weak endothermic event between 40 and 80 °C during the first heating scan, which is not apparent in the second heating scan. As suggested by the temperature-dependent SAXS analysis (Figure S1, Supporting Information), this endothermic event represents melting of the mesophase into an isotropic micellar solution. The latent heat associated with these endothermic events is of the order of 1–2 J g^{-1}, consistent with latent heat values for a liquid crystal phase to isotropic phase transition.[47] For the sample containing 65 wt% water (i.e., no PEGDA), this endothermic event is observed at 45.9 °C and likely represents melting of the discontinuous cubic phase into an isotropic state. As small amounts (5 or 10 wt%) of PEGDA are added to the system, this transition shifts to higher temperatures, and is observed at 65.9 °C for 10 wt% PEGDA, suggesting that the addition of PEGDA, up to 10 wt%, stabilizes the discontinuous cubic mesophase in these systems. However, at 20 wt% PEGDA this endotherm has shifted back to 49.5 °C, suggesting that further addition of PEGDA no longer stabilizes the discontinuous cubic mesophase.

While the system containing 35 wt% IL and 65 wt% water exhibits a discontinuous cubic phase; at 30 wt% IL and 70 wt% water, the cubic mesophase is disrupted and a micellar solution was observed instead.[41] This indicates that 65 wt% water is close to the maximum water content that the system can tolerate before disruption of the discontinuous cubic phase.[41] Therefore, it could be rationalized that substitution of 5 or 10 wt% water by PEGDA stabilizes the mesophase present by reducing the total amount of water. However, at 20 wt% PEGDA, there are insufficient amount of water molecules to effectively solvate the headgroup of the ionic liquid, therefore the melting point of the system decreases. This is consistent with the formation of a micellar solution, as suggested by the SAXS data at 30 wt% PEGDA.

In conclusion, both DSC and SAXS results suggest that PEGDA incorporation has little effect on the type of mesophase formed, although its thermal stability starts to decrease above 10 wt% PEGDA, before being completely disrupted at 30 wt% PEGDA.

3.1.2. Impact of Comonomer Chemistry

Since an optimum comonomer concentration of 20 wt% was determined for the C_{16}mimAcr/water/PEGDA systems, further investigation of the impact of comonomer chemistry was conducted at this concentration.

Figure 4 shows the SAXS patterns of 35/45/20 wt% C_{16}mimAcr/water/comonomer systems containing 20 wt% PEGDA, PEGDMA, HEA, and HEMA. Similarly to the PEGDA system, the SAXS pattern of the PEGDMA system exhibits a characteristic pattern of a discontinuous cubic phase, which could be indexed as a $Pm\bar{3}n$ lattice with up to 12 identified reflections. The lattice parameter, a, of the PEGDMA system is 100.4 Å. This value is slightly larger than the lattice parameter calculated for the PEGDA system (a: 97.5 Å). The smaller reduction of the lattice parameter for the PEGDMA system may indicate that the PEGDMA molecules are not only located at the headgroup interface, but also, may be slightly deeper in the hydrophobic domain,[44,45] possibly due to either the presence of the methacrylate functional group and/or the slightly smaller size of the of PEGDMA, allowing PEGDMA molecule to penetrate deeper in the hydrophobic domain (M_n = 400 and 575 for the PEGDMA and PEGDA, respectively).

The SAXS pattern of the HEA system also exhibits a pattern characteristic of a discontinuous cubic phase, which could be indexed as a $Pm\bar{3}n$ lattice with up to 15 identified reflections. Again, the SAXS pattern of the HEA-containing system is shifted to higher q values compared to that of the C_{16}mimAcr/water system. The lattice parameter, a, of the HEA system is 95 Å. This value is slightly smaller than the lattice parameter

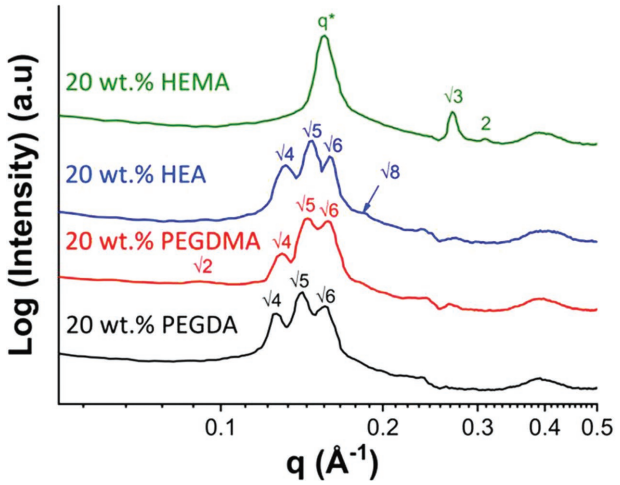

Figure 4. Integrated lab-SAXS patterns of 35/45/20 wt% C_{16}mimAcr/water/PEGDA system (black), 35/45/20 wt% C_{16}mimAcr/water/PEGDMA system (red), 35/45/20 wt% C_{16}mimAcr/water/HEA system (blue), and 35/45/20 wt% C_{16}mimAcr/water/HEMA system (green). Peak assignment for the main diffraction peaks is also included.

calculated for the PEGDA system, which was equal to 97.5 Å. This indicates a better packing of the HEA comonomer at the headgroup interface,[44,45] likely due to the difference in molecule size, when comparing PEG-based comonomer with HE-based comonomer.

Interestingly, the incorporation of HEMA results in a significant change of the SAXS pattern, indicating the presence of a 2D-hexagonal phase, with up to three identified reflections. The change in mesophase between the HEMA and HEA systems might be due to differences in the comonomer molecule location, with the HEMA molecules not only located at the headgroup interface, but also, slightly deeper in the hydrophobic domain.[44,45] This results in the formation of a different spontaneous curvature which would allow the accommodation of the new molecular arrangement, associated with the 2D-hexagonal phase. Similar observations, in terms of comonomer locations are made when comparing the PEGDA and PEGDMA systems, which could be attributed to the presence of the additional methyl group on the comonomer backbone. However, no mesophase change is observed in the PEGDMA system. This is likely due to both molecular size difference between the PEG-based and HE-based comonomers and a difference in the hydrophilic nature between the two comonomers (PEO chains), limiting the penetration of the comonomer into the hydrophobic domain. The formation of a polymerizable LLC system with a 2D-hexagonal phase is important for the incorporation/alignment of CPNs.[19]

To further investigate the impact of comonomer chemistry, DSC analysis was also performed to probe the thermal stability of the mesophase formed by the various C_{16}mimAcr/water/comonomer systems.

Figure 5 shows the first and second DSC heating scans of the 35/45/20 wt% C_{16}mimAcr/water/comonomer systems containing 20 wt% PEGDA, PEGDMA, HEA, or HEMA. DSC profiles of the systems with PEGDA and PEGDMA are quite comparable, as expected from their similar chemical structures. However, the weak endothermic event associated with the melting of the mesophase for the PEGDA system is shifted to higher temperature in the case of the PEGDMA system (i.e., 85.8 vs 49.5 °C for PEGDMA and PEGDA, respectively). This suggests that the discontinuous cubic phase present in the PEGDMA system is thermally more stable than that of the PEGDA system. This coincides with the observation of a shaper endothermic event at ≈–1 °C for the PEGDMA system, which is also slightly shifted to lower temperature, when compared to the PEGDA system. Overall, these results suggest that the discontinuous phase formed by the PEGDMA system is more ordered, resulting in enhanced thermal stability of the mesophase, when compared to the PEGDA system.

On the other hand, significant changes in the DSC profiles of the HE-based system (2-hydroxyethyl-based system) are observed compared to the PEG-based systems (poly(ethyleneglycol)-based system). A complex endothermic event is observed between −30 and 5 °C, likely representing the lamellar crystalline phase to lamellar gel phase transition and the lamellar gel phase to either a micellar or columnar mesophase transition. Unlike the systems containing PEG-based comonomer, the HE-based systems do not undergo any crystallization or glass transitions in the temperature range studied, supporting the conclusion that these transitions are

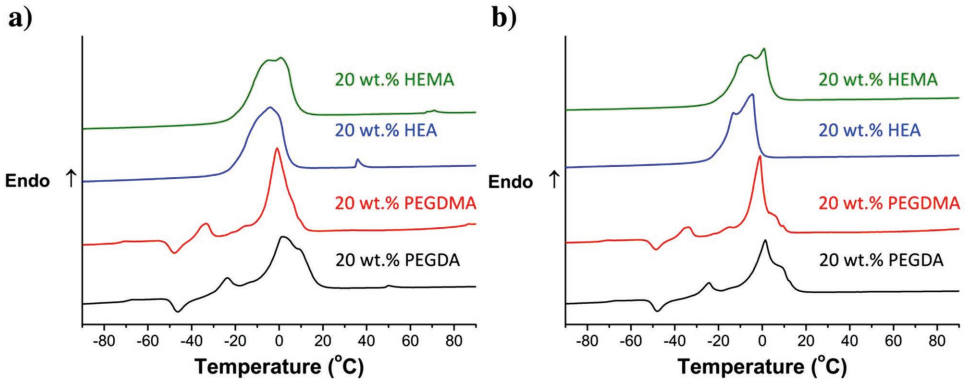

Figure 5. DSC heating profiles of 35/45/20 wt% C_{16}mimAcr/water/PEGDA (black), 35/45/20 wt% C_{16}mimAcr/water/PEGDMA (red), 35/45/20 wt% C_{16}mimAcr/water/HEA (blue), and of 35/45/20 wt% C_{16}mimAcr/water/HEMA (green); a) First heating scan and b) second heating scan.

associated to ethylene oxide chains present in PEG-based comonomers. A weak endothermic event, associated with the melting of the discontinuous cubic phase, is observed at 35.4 °C, for the HEA system.

It is clear from the DSC results that the chemistry of the comonomer has a significant impact on the thermal stability of the discontinuous cubic phase formed by the PEGDA, PEGDMA, and HEA systems. When comparing the PEGDA and PEGDMA systems, the use of the latter results in a drastic increase of the mesophase melting temperature, going from 49.5 to 85.8 °C for PEGDA and PEGDMA, respectively. For acrylate-based comonomers, the substitution of the PEGDA for the HEA comonomer results in a significant reduction of the mesophase melting temperature, going from 49.5 to 35.4 °C, respectively. The enhanced thermal stability of the PEGDA system is likely due to the entanglement of the ethylene oxide chain, as more energy is required to break the intermolecular polymer chain interaction.

The DSC results for the HEMA system, which is the only system exhibiting a 2D-hexagonal phase, are similar to those for the HEA system, with a complex endothermic event observed between −30 and 10 °C. However, a significant increase of the melting temperature of the mesophase to 70.4 °C is observed. In this case, it is not clear if the increase of the melting temperature of the mesophase is due to the formation of different mesophases and/or the introduction of a methyl group on the polymerizable moiety of the comonomer.

3.2. Post-Photopolymerization Characterization

Now that a better understanding of the impact of comonomer chemistry on the type of mesophase formed and their relative thermal stability has been established, the mesostructure retention of the C_{16}mimAcr/water/comonomer systems, post-photopolymerization, was assessed by SAXS.

3.2.1. Mesostructure Retention Study

Independent of the chemistry of the comonomer (i.e., PEGDA or PEGDMA) used or the mesophase present (e.g., polymerization temperature) prior to polymerization, all self-standing polymer formed by PEGDA or PEGDMA systems exhibit a similar SAXS pattern post-photopolymerization, suggesting both systems undergo structural rearrangement toward a similar nanostructure. On the other hand, the photopolymerization of the HE-based did not result in self-standing polymer film (see Supporting Information for details). **Figure 6**a shows an example of the SAXS pattern obtained by all C_{16}mimAcr/water/comonomer systems, in this case from the C_{16}mimAcr/water/PEGDA system with 20 wt% PEGDA, pre- and post-polymerization. The SAXS pattern post-polymerization has changed significantly compared to that prior to UV-exposure, suggesting that structural rearrangements are occurring during the photopolymerization. The post-polymerized SAXS pattern could be indexed as two different lamellar phases where $L_{\alpha 1}$, $q_1(100) = 0.165$ Å^{-1}, corresponding to a repeat distance $d = 2\pi/q = 38.1$ Å and $L_{\alpha 2}$, $q_1(100) = 0.190$ Å^{-1}, corresponding to a

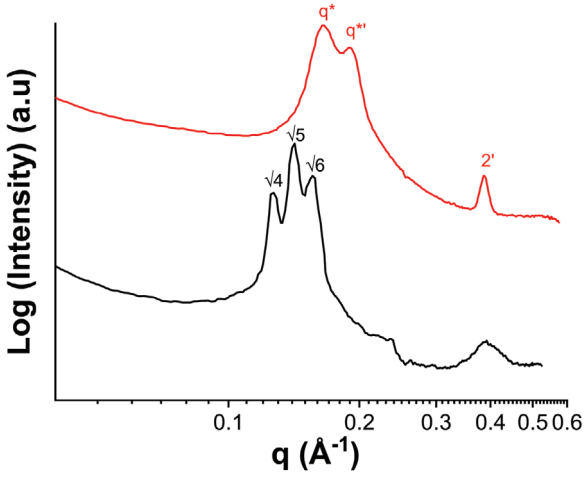

Figure 6. Integrated lab-SAXS patterns of 35/45/20 wt% C_{16}mimAcr/water/PEGDA; (black) pre- and (red) post-polymerization. The broad peak observed at 0.4 Å^{-1} for the pre-polymerization system is from the Kapton window of the capillary sample holder. A different sample holder without Kapton windows was used for the post-polymerization sample. Peak assignment for the main diffraction peaks is also included. Inset is a photograph of the 35/45/20 wt% C_{16}mimAcr/water/PEGDA post-polymerization.

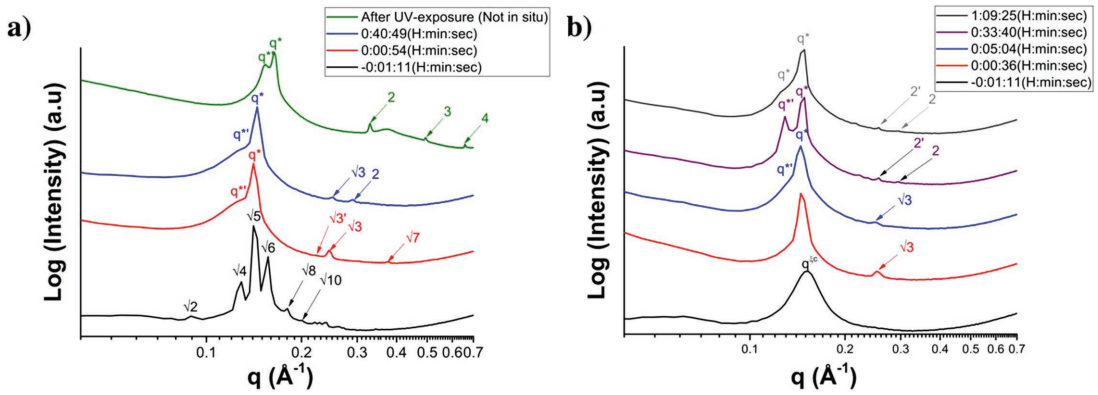

Figure 7. Time-resolved synchrotron-SAXS pattern of a C_{16}mimAcr/water/PEGDA sample containing 20 wt% of PEGDA during UV-exposure at a) 20 °C and b) 60 °C.

repeat distance $d = 2\pi/q = 33.1$ Å. The repeat distances of the two lamellar structures suggest the formation of an interdigitated bilayer configuration.[48,49] Additionally, the second-order diffraction peak of the second lamellar phase is observed at 0.386 Å^{-1}.

To better understand why these structure rearrangements occurred, in situ SAXS polymerization measurements have also been performed during the photopolymerization of the C_{16}mimAcr/water/PEGDA system containing 20 wt% PEGDA, due to its fast polymerization kinetics. **Figure 7** shows the synchrotron source SAXS patterns of the C_{16}mimAcr/water/PEGDA system during UV-exposure at 20 °C as well as for the post-polymerized sample. As described earlier, the SAXS pattern of the PEGDA system pre-polymerization suggests the formation of a discontinuous cubic phase. As can be seen in Figure 7a (brown line), a significant change in the SAXS pattern of the PEGDA-containing system is observed after only 54 s of UV-exposure with the appearance of an intense reflection centered at $q = 0.141$ Å^{-1}. This reflection has a clear lower q shoulder, which is centered at approximately 0.130 Å^{-1}. Three low intensity reflections were also observed at 0.220, 0.245, and 0.375 Å^{-1}. Surprisingly, the two lowest q reflections could be indexed along with the main reflection (i.e., 0.141 Å^{-1}) using the following relationship characteristic of a 2D-hexagonal phase: $q_1(100)$: $q_2(110)$: $q_3(210)$ = 1:√3:√7. On the other hand, the broad shoulder observed at 0.130 Å^{-1} shows a q_1/q_2 relationship equal to √3 with the reflection centered at 0.220 Å^{-1}. This relationship could be attributed to a 2D-hexagonal phase with a slightly larger lattice parameter, a, compared to that of the 2D-hexagonal phase indexed previously.

After 40 min of UV-exposure (blue line in Figure 7a), a similar indexation could be made, except for the extinction of the reflection centered at 0.375 Å^{-1} along with an additional reflection at 0.288 Å^{-1}. This additional reflection could be indexed with the main reflection peak centered at 0.144 Å^{-1}, giving the following relationship: $q_1(100)$: $q_2(110)$: $q_3(200)$ = 1:√3:√4, characteristic of a 2D-hexagonal phase. In contrast, no additional reflection could be associated with the lower q shoulder observed at 0.135 Å^{-1}.

The synchrotron source SAXS pattern of the PEGDA system acquired 1 week after polymerization (i.e., not in situ) is shown in Figure 7a (green line). A slight shift to higher q of the two main reflections is observed compared to the in situ condition, likely due to water loss. TGA measurement of the PEGDA system gave a water content of approximately 20 wt% immediately after 30 min UV-polymerization. After a week of storage, the sample reached an equilibrium water content of 10 wt%. In the SAXS pattern of the post-polymerized sample, five reflections are observed at 0.154, 0.164, 0.330, 0.493, and 0.657 Å^{-1}, which could be indexed as: $q_1(100)$: $q_2(200)$: $q_3(300)$: $q_4(400)$ = 1, 2, 3, and 4, indicating the presence of a lamellar phase. Although the lower q shoulder observed in the in situ condition appears more resolved for the post-polymerized sample, no additional reflections were observed which could be indexed. However, as the two most intense reflections were indexed to two similar phases with slightly different lattice parameters during the in situ measurement, it could be rationalized that the reflection centered at 0.154 Å^{-1} corresponds to the first-order diffraction of another lamellar phase. The structural changes observed between the end of in situ measurement and post-drying suggest that structural rearrangement also occurs during the drying period of the polymer.

Another in situ experiment was also performed at 60 °C to investigate the impact of polymerization temperature on structural rearrangement. Figure 7b shows the SAXS patterns of the C_{16}mimAcr/water/PEGDA system during UV-exposure at 60 °C. At this temperature, the PEGDA system exhibits only one broad reflection peak centered at 0.152 Å^{-1}, indicating the formation of a micellar phase (i.e., fluid sample). This is consistent with the observation of a weak endothermic event at 49.5 °C in the DSC traces of the PEGDA-containing system, which corresponded to the liquid crystalline phase melting into an isotropic state. After only 36 s of UV-exposure, the SAXS pattern again changes significantly with the appearance of two sharp reflections centered at 0.146 and 0.254 Å^{-1}, giving the following relationship characteristic of a 2D-hexagonal phase: $q_1(100)$: $q_2(110)$ = 1:√3. The structural rearrangement toward the formation of a 2D-hexagonal phase was also suggested by the in situ experiment on the PEGDA system at 20 °C. As the UV-exposure time increases, a clear lower q shoulder from the most intense reflection becomes more pronounced, resulting in a reflection peak centered at 0.129 Å^{-1} after 33 min of UV-exposure. Four reflections are observed at this time. The indexation of the SAXS pattern

suggests that the two most intense reflections centered at 0.129 and 0.149 $Å^{-1}$ represent the first-order diffraction peaks of two lamellar phases, with second-order reflections centered at 0.256 and 0.295 $Å^{-1}$, respectively. The formation of two lamellar phases was not observed during the in situ experiment on the PEGDA system at 20 °C, instead the SAXS data suggested the presence of two 2D-hexagonal phases. However, after a drying period of 1 week, the SAXS pattern of the PEGDA system polymerized at 20 °C also suggested the formation of two lamellar phases. No significant changes are observed in the SAXS patterns after 33 min of UV-exposure, apart from partial disappearance of the first reflection, suggesting that this lamellar phase is likely to be less ordered.

The sequence of structural changes, going from spherical micelle to cylindrical micelle and finally to a lamellar architecture, observed during the photopolymerization of the PEGDA-containing system, follows a typical order that is related to an increase in the critical packing parameter.[50] This parameter is a function of the hydrocarbon volume divided by the headgroup area and the critical chain length. The increase of the critical packing parameter is likely due to a reduction of headgroup area induced by cross-linking of the acrylate moiety.

4. Conclusions

Polymerizable LLC systems with intact alkyl chain bilayers for peptide-based channel inclusion, were developed using a polymerizable LLC and various comonomers. The impact of comonomer concentration on the mesophase originally formed by the C_{16}mimAcr/water/PEGDA system was characterized prior to photopolymerization by means of DSC and SAXS. The incorporation of 20 wt% PEGDA was found to be the optimum comonomer concentration in terms of mesophase preservation and polymerization kinetics, with the fabrication of a self-standing polymer membrane in only 30 min.

Additionally, the effect of comonomer chemistry on the phase behavior of C_{16}mimAcr/water/comonomer systems with a comonomer concentration of 20 wt% was investigated by substituting PEGDA with PEGDMA, HEA, or HEMA. The substitution of PEGDA for either PEGDMA or HEA had little impact on the type of mesophase formed pre-photopolymerization, in these cases, a discontinuous cubic phase. However, the chemistry of the comonomer has a significant impact on the thermal stability of the resulting mesophase, with thermal stability described as follows: HEA<PEGDA<PEGDMA. Interestingly, the use of HEMA comonomer triggers the formation of a 2D-hexagonal phase, likely due to difference in location of the comonomer molecules with respect to the headgroup interface.

Finally, post-photopolymerization SAXS analysis of the C_{16}mimAcr/water/comonomer systems suggests that the formation of two lamellar phases with slightly different repeat distances, is observed for all systems. In situ SAXS polymerization analysis highlights that the sequence of structural changes occurring during photopolymerization follows a typical order that is related to an increase in the critical packing parameter, likely due to a reduction of headgroup area induced by cross-linking of the acrylate moiety. These results provide a better understanding of the development of polymerizable LLC system, especially on the impact that the polymerizable moiety location has on the mesostructure retention during photopolymerization. It appears that having a polymerizable counterion is detrimental for the mesostructure retention, as rearrangement occurred during the cross-linking process. Future work will investigate the mesostructure retention of a polymerizable LLC system, where the polymerizable moiety is located on the cation headgroup. This could limit the reduction of headgroup area and still allow access of the alkyl chain bilayer for the incorporation of peptide-based channels.

Supporting Information

Supporting Information is available from the Wiley Online Library or from the author.

Acknowledgements

This work was supported by the Australian Research Council (ARC) through the Australian Laureate Fellowships FL110100013 (MF). The authors acknowledge funding for beamtime M9034 on the SAXS/WAXS beamline at the Australian Synchrotron, Victoria, Australia and the support from beamline scientists, Dr. Adrian Hawley and Dr. Nigel Kirby.

Conflict of Interest

The authors declare no conflict of interest.

Keywords

ionic liquids, nanostructured polymers, polymerizable lyotropic ionic liquid crystals

Received: July 18, 2018
Revised: September 19, 2018
Published online: October 30, 2018

[1] M. E. Tousley, X. Feng, M. Elimelech, C. O. Osuji, *ACS Appl. Mater. Interfaces* **2014**, *6*, 19710.
[2] D. L. Gin, J. E. Bara, R. D. Noble, B. J. Elliott, *Macromol. Rapid Commun.* **2008**, *29*, 367.
[3] B. R. Wiesenauer, D. L. Gin, *Polym. J.* **2012**, *44*, 461.
[4] R. Bouchet, S. Maria, R. Meziane, A. Aboulaich, L. Lienafa, J. P. Bonnet, T. N. T. Phan, D. Bertin, D. Gigmes, D. Devaux, R. Denoyel, M. Armand, *Nat. Mater.* **2013**, *12*, 452.
[5] T. Ichikawa, M. Yoshio, A. Hamasaki, J. Kagimoto, H. Ohno, T. Kato, *J. Am. Chem. Soc.* **2011**, *133*, 2163.
[6] M. Yoshio, T. Kagata, K. Hoshino, T. Mukai, H. Ohno, T. Kato, *J. Am. Chem. Soc.* **2006**, *128*, 5570.
[7] M. S. Mauter, M. Elimelech, C. O. Osuji, *ACS Nano* **2010**, *4*, 6651.
[8] P. W. Majewski, M. Gopinadhan, C. O. Osuji, *J. Polym. Sci., Part B: Polym. Phys.* **2012**, *50*, 2.
[9] X. Feng, M. E. Tousley, M. G. Cowan, B. R. Wiesenauer, S. Nejati, Y. Choo, R. D. Noble, M. Elimelech, D. L. Gin, C. O. Osuji, *ACS Nano* **2014**, *8*, 11977.
[10] R. C. Smith, W. M. Fischer, D. L. Gin, *J. Am. Chem. Soc.* **1997**, *119*, 4092.

[11] R. Klein, G. J. T. Tiddy, E. Maurer, D. Touraud, J. Esquena, O. Tache, W. Kunz, *Soft Matter* **2011**, *7*, 6973.
[12] G. Zhang, X. Chen, Y. Zhao, Y. Xie, H. Qiu, *J. Phys. Chem. B* **2007**, *111*, 11708.
[13] X. Auvray, C. Petipas, R. Anthore, I. Rico, A. Lattes, *J. Phys. Chem.* **1989**, *93*, 7458.
[14] S. Grubjesic, S. Seifert, M. A. Firestone, *Macromolecules* **2009**, *42*, 5461.
[15] R. Chapman, M. Danial, M. L. Koh, K. A. Jolliffe, S. Perrier, *Chem. Soc. Rev.* **2012**, *41*, 6023.
[16] M. R. Ghadiri, J. R. Granja, L. K. Buehler, *Nature* **1994**, *369*, 301.
[17] J. R. Granja, M. R. Ghadiri, *J. Am. Chem. Soc.* **1994**, *116*, 10785.
[18] J. Zhu, J. Cheng, Z. Liao, Z. Lai, B. Liu, *J. Comput.-Aided Mol. Des.* **2008**, *22*, 773.
[19] N. Byrne, D. Menzies, N. Goujon, M. Forsyth, *Chem. Commun.* **2013**, *49*, 7729.
[20] D. L. Gin, W. Gu, B. A. Pindzola, W.-J. Zhou, *Acc. Chem. Res.* **2001**, *34*, 973.
[21] M. A. DePierro, C. A. Guymon, *Macromolecules* **2014**, *47*, 5728.
[22] F.-G. Wu, N.-N. Wang, Q.-G. Zhang, S.-F. Sun, Z.-W. Yu, *J. Colloid Interface Sci.* **2012**, *374*, 197.
[23] L. Wang, X. Chen, Y. Chai, J. Hao, Z. Sui, W. Zhuang, Z. Sun, *Chem. Commun.* **2004**, *0*, 2840.
[24] M. U. Araos, G. G. Warr, *J. Phys. Chem. B* **2005**, *109*, 14275.
[25] K. S. Worthington, C. Baguenard, B. S. Forney, C. A. Guymon, *J. Polym. Sci., Part B: Polym. Phys.* **2017**, *55*, 471.
[26] B. P. Hoag, D. L. Gin, *Macromolecules* **2000**, *33*, 8549.
[27] J. Zhang, Z. Xie, A. J. Hill, F. H. She, A. W. Thornton, M. Hoang, L. X. Kong, *Soft Matter* **2012**, *8*, 2087.
[28] C. L. Lester, C. D. Colson, C. A. Guymon, *Macromolecules* **2001**, *34*, 4430.
[29] D. Batra, S. Seifert, L. M. Varela, A. C. Y. Liu, M. A. Firestone, *Adv. Funct. Mater.* **2007**, *17*, 1279.
[30] R. Thundathil, J. O. Stoffer, S. E. Friberg, *J. Polym. Sci.: Polym. Chem. Ed.* **1980**, *18*, 2629.
[31] D. H. Gray, S. Hu, E. Juuang, D. L. Gin, *Adv. Mater.* **1997**, *9*, 731.
[32] R. L. Kerr, S. A. Miller, R. K. Shoemaker, B. J. Elliott, D. L. Gin, *J. Am. Chem. Soc.* **2009**, *131*, 15972.
[33] Y.-S. Lee, J.-Z. Yang, T. M. Sisson, D. A. Frankel, J. T. Gleeson, E. Aksay, S. L. Keller, S. M. Gruner, D. F. O'Brien, *J. Am. Chem. Soc.* **1995**, *117*, 5573.
[34] W. Srisiri, A. Benedicto, D. F. O'Brien, T. P. Trouard, G. Orädd, S. Persson, G. Lindblom, *Langmuir* **1998**, *14*, 1921.
[35] W. Srisiri, T. M. Sisson, D. F. O'Brien, K. M. McGrath, Y. Han, S. M. Gruner, *J. Am. Chem. Soc.* **1997**, *119*, 4866.
[36] B. A. Pindzola, B. P. Hoag, D. L. Gin, *J. Am. Chem. Soc.* **2001**, *123*, 4617.
[37] D. Batra, S. Seifert, M. A. Firestone, *Macromol. Chem. Phys.* **2007**, *208*, 1416.
[38] C. L. Lester, C. A. Guymon, *Polymer* **2002**, *43*, 3707.
[39] B. A. Pindzola, J. Jin, D. L. Gin, *J. Am. Chem. Soc.* **2003**, *125*, 2940.
[40] M. A. Firestone, J. A. Dzielawa, P. Zapol, L. A. Curtiss, S. Seifert, M. L. Dietz, *Langmuir* **2002**, *18*, 7258.
[41] N. Goujon, M. Forsyth, L. F. Dumee, G. Bryant, N. Byrne, *Phys. Chem. Chem. Phys.* **2015**, *17*, 23059.
[42] G. A. Becht, M. Sofos, S. Seifert, M. A. Firestone, *Macromolecules* **2011**, *44*, 1421.
[43] Z. Yi, L. F. Dumée, C. J. Garvey, C. Feng, F. She, J. E. Rookes, S. Mudie, D. M. Cahill, L. Kong, *Langmuir* **2015**, *31*, 8478.
[44] I. Kayali, K. Qamhieh, B. Lindman, *J. Dispersion Sci. Technol.* **2006**, *27*, 1151.
[45] M. H. Uddin, N. Kanei, H. Kunieda, *Langmuir* **2000**, *16*, 6891.
[46] S. Sasaki, *J. Phys. Chem. B* **2007**, *111*, 2473.
[47] P. J. Collings, M. Hird, *Introd. to Liq. Cryst. Chem. Phys.*, Taylor and Francis, Oxfordshire, UK **1997**, 0-312.
[48] A. E. Bradley, C. Hardacre, J. D. Holbrey, S. Johnston, S. E. J. McMath, M. Nieuwenhuyzen, *Chem. Mater.* **2002**, *14*, 629.
[49] A. Downard, M. J. Earle, C. Hardacre, S. E. J. McMath, M. Nieuwenhuyzen, S. J. Teat, *Chem. Mater.* **2004**, *16*, 43.
[50] J. N. Israelachvili, *Intermol. Surf. Forces*, 3rd Ed., Academic Press, Cambrigde, MA, USA **2011**, 0-710.